

REVIEW ARTICLE

Towards a random laser with cold atoms

W. Guerin¹, N. Mercadier¹, F. Michaud¹‡, D. Brivio¹§,
L. S. Froufe-Pérez², R. Carminati³, V. Ereemeev⁴,
A. Goetschy⁴, S. E. Skipetrov⁴, R. Kaiser¹

¹ Institut Non Linéaire de Nice, CNRS and Université de Nice Sophia-Antipolis,
1361 route des Lucioles, 06560 Valbonne, France

² Instituto de Ciencia de Materiales de Madrid, CSIC, Sor Juana Inés de la
Cruz 3, Cantoblanco, Madrid 28049, Spain

³ Institut Langevin, ESPCI ParisTech, CNRS, Laboratoire d'Optique Physique,
10 rue Vauquelin, 75231 Paris Cedex 05, France

⁴ Université Joseph Fourier, Laboratoire de Physique et Modélisation des
Milieux Condensés, CNRS, 25 rue des Martyrs, 38042 Grenoble, France

E-mail: William.Guerin@inln.cnrs.fr

PACS numbers: 37.30.+i,42.25.Dd,42.55.Zz

Submitted to: *J. Opt. A: Pure Appl. Opt.*

Abstract. Atoms can scatter light and they can also amplify it by stimulated emission. From this simple starting point, we examine the possibility of realizing a random laser in a cloud of laser-cooled atoms. The answer is not obvious as both processes (elastic scattering and stimulated emission) seem to exclude one another: pumping atoms to make them behave as amplifier reduces drastically their scattering cross-section. However, we show that even the simplest atom model allows the efficient combination of gain and scattering. Moreover, supplementary degrees of freedom that atoms offer allow the use of several gain mechanisms, depending on the pumping scheme. We thus first study these different gain mechanisms and show experimentally that they can induce (standard) lasing. We then present how the constraint of combining scattering and gain can be quantified, which leads to an evaluation of the random laser threshold. The results are promising and we draw some prospects for a practical realization of a random laser with cold atoms.

Keywords: Random laser, cold atoms

‡ Present address: LNE-SYRTE, CNRS UMR 8630, UPMC, Observatoire de Paris, 61 rue de l'Observatoire, 75014 Paris, France

§ Present address: Dipartimento di Fisica, Università di Milano, I-20113, Italy

1. Introduction: atoms as scatterers and amplifiers

Among atom-light interactions, elastic – or Rayleigh – scattering is one of the simplest processes [1]. It has been known for a long time that in optically thick atomic vapors, multiple scattering leads to diffusion of light, or “radiation trapping” [2, 3]. However, only the progress in laser cooling and trapping [4] allowed the more recent demonstration and study of this effect with only true elastic scattering, by suppressing the Doppler-induced frequency redistribution [5, 6, 7]. Many experiments have also been performed to study the coherence properties of multiply-scattered light in such a medium, especially using coherent backscattering as a probe [8, 9] (see [10, 11, 12, 13] for review articles devoted to this topic).

Cold atoms have also driven a renewed interest in non linear spectroscopy, as the suppression of Doppler broadening allows the resolution of narrow spectral resonances in pump-probe spectroscopic schemes [14]. One example is Raman gain between Zeeman sublevels [15, 16]. The idea of building a laser upon this gain followed soon after its first observation [17]. Nevertheless, cold atoms in optical cavity have been then mainly used for quantum optics purposes [18] and laser demonstrations with different gain mechanisms are much more recent [19, 20].

If one could combine both gain and radiation trapping at the same time in a cold atom cloud, this could give rise to a diffusive random laser, as predicted by Letokhov [21]. Since his original “photonic bomb” prediction, great efforts have been made to experimentally demonstrate this effect in different kinds of systems [22, 23, 24, 25, 26, 27, 28], as well as to understand the basic properties of random lasing [29, 30, 31, 32]. The broad interest of this topic is driven by potential applications (see [33] and references therein) and by its connection to the fascinating subject of Anderson localization [34, 35]. State-of-the-art random lasers [33, 36, 37, 38] are usually based on condensed matter systems, and feedback is provided by a disordered scattering medium, while gain is provided by an active material lying in the host medium or inside the scatterers. In general, scattering and gain are related to different physical entities.

The peculiarity of a random laser based on cold atoms would be that the same microscopic elements (the atoms) would provide both ingredients (scattering and gain) of random lasing. On the one hand, it leads to an easier characterization and modelling of the microscopic properties of the system, which can be extremely valuable for a better understanding of the physics of random lasers. Moreover, cold atoms are “clean” and perfectly characterized samples. In addition, relaxation of optical coherences is limited by radiative processes, which makes the transition to cooperative emission, such as superfluorescence [39, 40], more accessible than in condensed matter systems. On the other hand, it is clear that pumping atoms to induce gain reduces drastically their scattering cross-section, due to the saturation effect [1]: atoms spend less time in their ground state, in which they can scatter light. It is thus not obvious at all that reasonable conditions for random lasing can be obtained in cold atoms. Moreover, these conditions are expected to be different for each gain mechanism.

The purpose of this article is to present the status of our experimental and theoretical investigations on this issue. In the next section we present our work on lasing with cold atoms, with a standard cavity [20]. Experimentally, this demonstration of a cold-atom-based laser with different gain mechanisms is a first important step towards the building of a random laser. More fundamentally, this experiment can be compared to theory to validate or improve the modelling of such

gain media, including saturation effect, laser dynamics or statistics. We present a part of this modelling in section 3. Ultimately, when studying the random laser properties, it will be of first importance to be able to discriminate which behaviour originates from the particular used gain medium and mechanism and which one is specific to the feedback mechanism (standard cavity or scattering). The cavity-laser thus serves as a reference, to be compared with theory and with the (forthcoming) random laser.

The second important step of this project, presented in section 4, is to quantify the constraint of combining gain and scattering at the same time. This leads to the evaluation of the random laser threshold [41, 42]. The goal is first to establish the feasibility of a random laser with cold atoms, which was not obvious, and second to compare the different gain mechanisms in order to experimentally choose the more appropriate one with the best pumping parameters. This is necessary before conducting further experimental efforts to achieve the threshold. As the results are promising, we draw some prospects for our future work in the last section.

2. Gain and lasing with cold atoms: experimental investigation

In this section, we briefly describe our experimental setup and then the different gain mechanisms we have studied. Mollow gain is the simplest as it involves only one pumping field and two-level atoms [43, 44]. By using the more complex atomic structure of rubidium atoms, we can create two-photon transitions between two non-degenerate ground states. This can produce Raman gain [15, 16, 17]. Finally, the atomic non-linearity can give rise to parametric gain, for example with four-wave mixing. We have demonstrated laser action with each of these mechanisms (figure 1) [20]. We mention also briefly some other gain mechanisms that could be used.

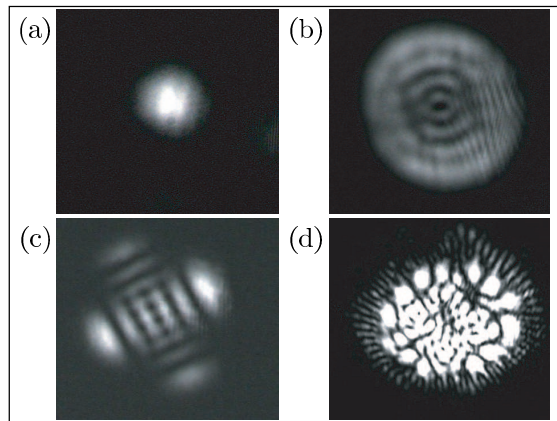


Figure 1. Transverse modes of cold-atom lasers. (a) Gaussian TEM₀₀ mode, obtained by inserting a small diaphragm in the cavity. Typical modes of: (b) the Mollow laser, (c) the Raman laser, and (d) the four-wave mixing laser respectively.

2.1. Experimental setup

Our experiment uses a cloud of cold ⁸⁵Rb atoms confined in a vapour-loaded Magneto-Optical Trap (MOT) [4] produced by six large independent trapping beams, allowing the trapping of up to 10¹⁰ atoms at a density of 10¹⁰ atoms/cm³, corresponding

to an on-resonance optical thickness $b_0 \sim 10$. A linear cavity, formed by two mirrors separated by a distance $L = 0.8$ m, is placed outside the vacuum chamber. Reflections on the vacuum cell yields a low finesse $\mathcal{F} = 16$. To add gain to our system, we use either one or two counter-propagating pump beams, denoted F (forward) and B (backward), produced from the same laser with a waist $w_{\text{pump}} = 2.6$ mm, with linear parallel polarizations and a total available power $P = 80$ mW, corresponding to a maximum pump intensity $I = 2P/(\pi w_{\text{pump}}^2) \approx 750$ mW/cm². The pump is tuned near the $F = 3 \rightarrow F' = 4$ cycling transition of the $D2$ line of ⁸⁵Rb (frequency ω_0 , wavelength $\lambda = 780$ nm, natural linewidth $\Gamma/2\pi = 6.1$ MHz), with an adjustable detuning $\Delta = \omega_{F,B} - \omega_0$ and has an incident angle of about 20° with the cavity axis. An additional beam P is used as a local oscillator to monitor the laser spectrum or as a weak probe to measure transmission or reflection spectra (figures 4(b) and 5(b)) with a propagation axis making an angle with the cavity axis smaller than 10° . Its frequency ω_P can be swept around the pump frequency with a detuning $\delta = \omega_P - \omega_{F,B}$. Both lasers, pump and probe, are obtained by injection-locking of a common master laser, which allows to resolve narrow spectral features. In our experiments, we load a MOT for 29 ms, and then switch off the trapping beams and magnetic field gradient during 1 ms, when lasing or pump-probe spectroscopy are performed. In order to avoid optical pumping into the dark hyperfine $F = 2$ ground state, a repumping laser is kept on all time.

2.2. Gain mechanisms

2.2.1. Mollow gain The most simple gain mechanism we can imagine in cold atoms was described by Mollow [43] and observed soon afterwards [44]. It involves a two-level atom and one strong pumping field. Amplification comes from a three-photon transition from the ground state to the excited state via two absorptions of pump photons (figure 2(a)). This process can also be described in the dressed-state basis [1], in which a population inversion occurs (figure 7(a)).

The main amplification feature appears for a pump-probe detuning $\delta = \text{sign}(\Delta)\sqrt{\Delta^2 + \Omega^2}$, where Ω is the Rabi frequency of the pump-atom coupling, related to the pump intensity I by $\Omega^2 = \mathcal{C}^2\Gamma^2 I/(2I_{\text{sat}})$ ($I_{\text{sat}} = 1.6$ mW/cm² is the saturation intensity and \mathcal{C} is the averaged squared Clebsch-Gordan coefficient of the $F = 3 \rightarrow F' = 4$ transition) and has a typical width on the order of Γ . Note that another, dispersion-like feature appears around $\delta = 0$, which is associated with two-photon

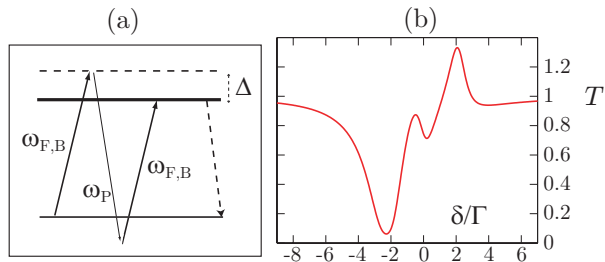


Figure 2. (a) Principle of the Mollow gain depicted as a three-photon transition from the ground state to the excited state. It can also be viewed as a population inversion in the dressed-state basis (figure 7(a)). (b) Transmission spectrum, computed for typical experimental parameters $b_0 = 10$, $\Omega = 2\Gamma$ and $\Delta = \Gamma$.

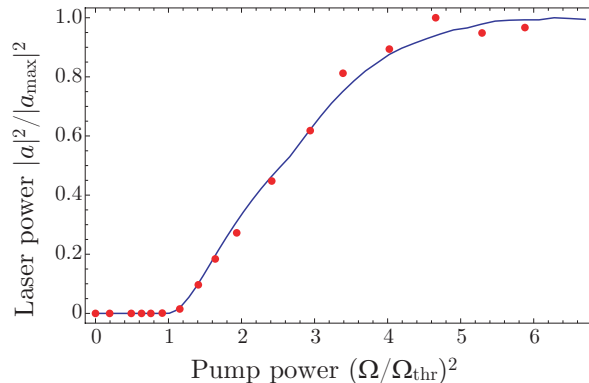


Figure 3. Laser power versus pump power. Points are experimental data obtained after an average of 1000 experiments, the continuous line is the theoretical fit (see section 3) with a single fit parameter $\eta \simeq 8$ (corresponding to $N \sim 10^8$ atoms in the cavity mode) and all other parameters fixed at their experimental values, $b_0 = 11$, $\Delta = \Gamma$, $\mathcal{F} = 16$, $L = 0.8$ m, and cavity waist at the MOT location $w = 500$ μm . The horizontal axis is normalized by the threshold value of the squared Rabi frequency Ω_{thr}^2 ; the vertical axis is normalized by the maximum value of the electromagnetic field intensity reached at about $(\Omega/\Omega_{\text{thr}})^2 \sim 5$.

spontaneous emission processes [45]. This contribution also induces gain but with a much smaller amplitude. Note that this can generate lasing without population inversion [46, 47, 48].

In our experiment, we have measured single-pass gain as high as 50 %, which is more than enough to induce lasing even with a low-finesse cavity [20]. This Mollow laser has an output intensity reaching 35 μW achieved for $|\Delta| \sim 2\Gamma$. Its threshold in pump intensity is in agreement with the corresponding measured single-pass gain and the losses of the cavity. The laser polarization is linear, parallel to the pump polarization, because this is the configuration for which gain is maximum, as the driven atomic dipole is then parallel to the probe field. We have also measured the output power as a function of the pump intensity, as reported in figure 3. We observe a threshold and the maximum intensity is reached for a pump power about 5 times larger than at the threshold. This behaviour is well described by the theoretical model presented in section 3.

The Mollow laser works for pump detuning $|\Delta| < 4\Gamma$. When the pump frequency is detuned farther away from the atomic resonance, Raman gain becomes dominant, and the system switches to another regime of laser, based on Raman gain.

2.2.2. Raman gain Raman gain relies on the pump-induced population inversion among the different light-shifted m_F Zeeman sublevels of the $F = 3$ hyperfine level [15, 16], as depicted in figure 4(a). The optical pumping induced by the π -polarized pump laser leads to a symmetric distribution of population with respect to the $m_F = 0$ sublevel of the ground state, with this sublevel being the most populated and also the most shifted, due to a larger Clebsch-Gordan coefficient [49]. To record a transmission spectrum, atoms are probed with a π -polarized (with perpendicular direction) probe beam, thus inducing $\Delta m_F = \pm 1$ Raman transitions. Depending on the sign of the pump-probe detuning δ , the population imbalance induces gain or absorption. Each

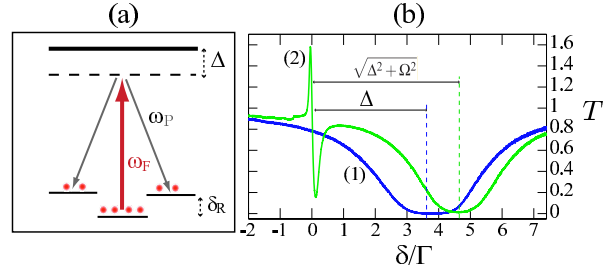


Figure 4. (a) Principle of the Raman mechanism, depicted here for a $F = 1 \rightarrow F' = 2$ transition. (b) Experimental transmission spectra, plotted as a function of the pump-probe detuning δ . Without pumping, spectrum (1) shows only the atomic absorption. A pump beam of detuning $\Delta = -3.8 \Gamma$ and intensity 13 mW/cm^2 , corresponding to a Rabi frequency $\Omega = 2.5 \Gamma$, is added to obtain spectrum (2), which then exhibits a Raman resonance in the vicinity of $\delta = 0$. Moreover, the atomic absorption is shifted due to the pump-induced light shift and the absorption is reduced due to saturation.

pair of neighboring sublevels contributes with a relative weight depending on the population inversion. In practice however, the contributions of different pairs are not resolved and only two structures (with opposite signs) are visible, one corresponding to amplification for $\delta = -\delta_R$ and one to absorption for $\delta = \delta_R$. Note that this situation corresponds to a red detuning for the pump ($\Delta < 0$) and that the signs are inverted for blue-detuning ($\Delta > 0$). As δ_R comes from a differential light-shift (because of different Clebsch-Gordan coefficients), it is usually on the order of $\Gamma/10$, whereas Δ is a few Γ . The width γ of the resonances is related to the elastic scattering rate, also much smaller than Γ [16]. Far from the main atomic absorption resonance, the Raman resonance is thus a narrow spectral feature, as in figure 4(b)

The laser obtained with Raman gain has an output polarization orthogonal to the pump one (contrary to the Mollow laser) and less power ($2 \mu\text{W}$). Moreover, the sharpness of the gain curve makes the Raman gain very sensible to any Doppler shift. The radiation pressure from the pump beam makes thus the laser emission to stop after only $\sim 20 \mu\text{s}$. On the other hand, the narrow spectrum of the laser can be easily characterized by a beat-note experiment [20].

2.2.3. Parametric gain The Mollow and Raman lasers only require one pump beam. By using a second pump beam, we can induce four wave mixing (FWM): the two pumps of frequencies ω_F and ω_B and one probe – or initial fluctuation – of frequency ω_P generate a fourth field at frequency ω_C , called the conjugate field [50, 51, 52]. The frequencies and wave-vectors of all the fields are related by energy and momentum conservations. If we want to obtain *gain* for the probe, we have to choose a configuration where the conjugate frequency equals the probe one: $\omega_C = \omega_P$. Then, the pump frequencies have to fulfill the condition $\omega_F + \omega_B = 2\omega_P$. From an experimental point of view, the most simple configuration consists of all frequencies to be the same (“degenerate FWM”). This is the experimental situation that we have studied so far, and we did obtain lasing in cold atoms with this mechanism [20]. Note that this mechanism has been observed a long time ago with hot atoms [53, 54, 55].

Due to the phase matching condition, however, the gain is not in the forward transmission of the probe beam, but in backward reflection, provided that the two

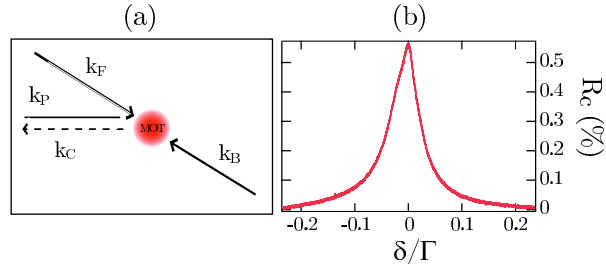


Figure 5. (a) Principle of four-wave mixing. (b) Typical experimental reflection spectrum.

pumps are counterpropagating. The conjugate beam is actually the phase-conjugate of the probe beam. This property has a number of consequences for the laser [20]. First, it leads to a different threshold condition [54]: a reflectivity of only 1 % is enough to generate lasing, despite the much larger losses of the cavity (32 % for a round trip). This is due to constructive interferences between transmitted and reflected waves, as observed in double-pass experiments [56]. Second, it leads to more complex transverse modes (figure 1(d)), because the phase conjugation mechanism allows any transverse pattern to be stable through the resonator [57].

Finally, these properties lead to a much larger power than with Mollow and Raman gain, as up to 300 μW have been obtained. Moreover, this laser might find application for other topics like pattern formation [58, 59] or the production of twin beams for quantum optics [60, 61] and even quantum imaging [62]. Note also that the use of two pump beams allows a longer laser emission (figure 6(b)) because the effect of radiation pressure on the cloud is suppressed (other effects can arise due to the dipole force, see [63]).

2.2.4. Other gain mechanisms Our previous study on the gain mechanisms that can be used in cold atoms is not exhaustive. For example, the two hyperfine ground states of rubidium atoms can also be used to produce Raman gain [64].

Other, more complicated, schemes, involve quantum interference to induce gain without population inversion (whatever the basis) [48]. This can be realized with a Λ scheme [65] or a V scheme [66, 67]. In this last configuration, a large detuning between the pump and the gain frequency can be reached by using the two D lines of rubidium, whose separation is 15 nm. If used to produce a random laser, this can be highly valuable to make the detection easier (see the discussion of section 5).

Another possibility is to use the atomic external degrees of freedom, i.e., their kinetic energy. Transitions between different velocity classes produce recoil-induced resonances [68], and high gain can be achieved [69]. These resonances can ultimately lead to a “Collective atomic recoil laser” [70, 71], which has been demonstrated with cold atoms [19].

Finally, one could also consider higher-order photonic processes, such as two-photon dressed-state lasers [72].

2.3. Laser dynamics

We have been interested so far only in steady-state properties. Our cold-atom-based laser could also reveal interesting dynamical properties.

For example, we have observed that the Mollow laser switches on very quickly, whereas the FWM laser switches on very slowly (figure 6 – notice the change in the time scales). The laser rise-times are related to the spectral properties of the gain mechanism. We are indeed in the bad cavity limit, where the decay rate of the cavity is not smaller than the spectral width of the amplification. The measured orders of magnitude ($\sim 0.2 \mu\text{s}$ for the Mollow laser, more than $100 \mu\text{s}$ for the FWM laser) are consistent with the inverse of the laser spectral width (a few MHz for the Mollow laser, a few kHz for the FWM laser). Note that the spectral width of the FWM laser, measured by a beating with a local oscillator (inset of figure 6(b) – note the logarithmic scale), is substantially smaller than the width of the reflectivity spectrum (figure 5(b)).

Clearly, further experimental and theoretical studies would be needed to fully understand the dynamical behaviour of these different lasers. However, a first insight is given in the next section.

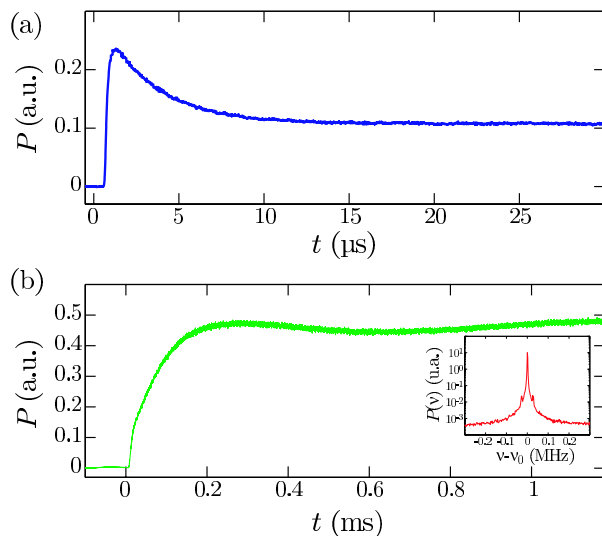


Figure 6. Temporal evolution of the Mollow (a) and FWM lasers (b). The pump beams are switched on at $t = 0$. Note the change in the time scales. The Mollow laser switches on very fast (the initial decrease is due to optical pumping to the dark hyperfine state), whereas the FWM laser needs more time. Inset of (b): Power spectrum, with a logarithmic scale, of the FWM laser measured by a beating with a local oscillator of frequency ν_0 . All data are the result of an average of 1000 cycles.

3. Model of the Mollow laser

We present in this section a theoretical analysis of our cold-atom laser based on Mollow gain.

3.1. Formalism

We consider an ensemble of N identical two-level atoms pumped by a strong field of frequency ω_L , detuning Δ and intensity characterized by the Rabi frequency Ω . They are placed inside a cavity of eigenfrequencies ω_m , and a_m , a_m^\dagger are the annihilation and creation operators, corresponding to the mode m . The cavity is partly open and the energy of the electromagnetic field can escape at a rate 2κ . We recall that we are in the bad cavity limit [73].

To describe the dynamics of the coupled system of atoms and modes of the electromagnetic field, we use the master equation approach [1, 73, 74]. The density matrix operator obeys

$$\dot{\rho} = -i [H, \rho] + L_A \rho + L_F \rho, \quad (1)$$

where we set $\hbar = 1$ and the Hamiltonian is

$$H = \frac{1}{2} \sum_{j=1}^N \left[-\Delta \cdot \sigma_{3j} + \Omega (\sigma_j + \sigma_j^\dagger) + \sum_m^M (g_{jm} \sigma_j^\dagger a_m + h.c.) \right] + \sum_{m=1}^M \delta_m a_m^\dagger a_m. \quad (2)$$

Here the rotating-wave approximation was used and the operators σ_{3j} , σ_j^\dagger and σ_j are standard Pauli matrices, describing the populations (σ_{3j}) and the coherences (σ_j) of the j -th atom. The detuning of the mode frequency from the pump frequency is δ_m and g_{jm} are the coupling constants between atoms and cavity modes, which we assume to be independent of the mode index m and to have the same absolute value g for all atoms and random phases ϕ_j : $g_{jm} = g \exp(i\phi_j)$. In the Hamiltonian of equation (2), only a part of modes of the electromagnetic field in the cavity (M modes) are treated explicitly, whereas spontaneous emission into other modes is taken into account through the first non-Hamiltonian term of the master equation (1):

$$L_A \rho = \frac{\Gamma}{2} \sum_{j=1}^N \left(2\sigma_j \rho \sigma_j^\dagger - \sigma_j^\dagger \sigma_j \rho - \rho \sigma_j^\dagger \sigma_j \right). \quad (3)$$

The second non-Hamiltonian term in equation (1) describes cavity damping of the electromagnetic modes:

$$L_F \rho = \kappa \sum_{m=1}^M \left(2a_m \rho a_m^\dagger - a_m^\dagger a_m \rho - \rho a_m^\dagger a_m \right). \quad (4)$$

The physical processes described by the set of equations (1–4) become especially clear in the dressed-state basis [1]. The dressed states are eigenstates of the system “atoms + pump field”. In the dressed-state basis, the states $|1\rangle_j$ and $|0\rangle_j$ of the two-level atom j become $|+\rangle_j = (\cos \theta) |1\rangle_j + (\sin \theta) |0\rangle_j$ and $|-\rangle_j = -(\sin \theta) |1\rangle_j + (\cos \theta) |0\rangle_j$, respectively, where $\Omega = \Omega' \sin 2\theta$ and $\Delta = -\Omega' \cos 2\theta$ with $\Omega' = \sqrt{\Omega^2 + \Delta^2}$ being the generalized Rabi frequency (figure 7(a)). Equations (2) and (3) can then be transformed (equation (4) remains unchanged) and equation (1) leads to the following semi-classical equations for quantum-mechanical expectation values of operators σ_j , σ_{3j} and a_m [73, 74]:

$$\dot{\sigma}_{3j} = -\gamma_1 (\sigma_{3j} - \bar{\sigma}_{3j}) + \Phi(\sigma_j, a_m), \quad (5)$$

$$\dot{\sigma}_j = -(\gamma_2 + i\Omega) \sigma_j + \Psi(\sigma_j, \sigma_{3j}, a_m), \quad (6)$$

$$\dot{a}_m = -(\kappa + i\delta_m) a_m + \Theta(\sigma_{3j}, \sigma_j), \quad (7)$$

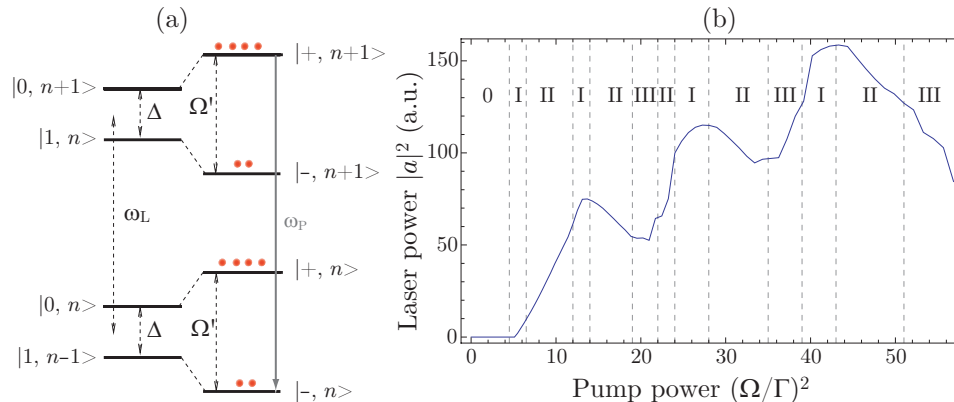


Figure 7. (a) Coupling of the bare atomic states $|0, n\rangle$, $|1, n\rangle$ (left) to the dressed states $|-, n\rangle$, $|+, n\rangle$ (right), where n stands for the number of pump photons. The population inversion and the subsequent gain is sketched on the dressed-state representation. (b) Laser power versus pump power for a laser with a single cavity mode interacting with atoms ($M = 1$). Values of parameters are chosen as in the experiment, $b_0 = 11$, $\Delta = \Gamma$, $\mathcal{F} = 16$, $L = 0.8$ m, $w = 500$ μm , and we have taken $\eta \simeq 15$, corresponding to $N = 2.3 \times 10^8$. $\delta_m = 1.8\Gamma$ is chosen at the maximum of the measured gain curve. Regions I, II and III correspond to three different types of behaviour illustrated in figure 8. Regions III (chaotic behaviour) appear only when η is large enough. (i.e., no chaotic behaviour is observed for $\eta = 8$ as in figure 3).

where $\bar{\sigma}_{3j} = -2 \cos 2\theta / (1 + \cos^2 2\theta)$, $\gamma_1 = (\Gamma/2) (1 + \cos^2 2\theta)$, $\gamma_2 = (\Gamma/4) (2 + \sin^2 2\theta)$ and the expressions of functions Φ , Ψ , Θ are given in Appendix A. The equations for σ_j^* and a_m^* are complex conjugates of equations (6) and (7), respectively. These equations describe respectively the evolution of the populations, the coherences and the cavity field. The first term of each right-hand-side contains the natural evolution associated with rates γ_1 , γ_2 and κ as well as the driving by the pump field (Rabi frequency Ω). The equations are coupled by their second terms (equations A.1–A.3), which contain the atom-field coupling g and the atom number N coupled to the cavity mode, which are in the mode of the cavity. For a Gaussian cavity mode with waist w one obtains [75] $g \simeq \sqrt{3c\Gamma/L}/k_0 w$, $N \simeq (k_0 w)^2 b_0 / 12$ where $k_0 = \omega_0/c = 2\pi/\lambda$, b_0 is the optical thickness of the cloud at resonance without pump and L the length of the cavity. To take into account the fact that volumes and shapes of the atomic cloud and cavity modes are different and not Gaussian, we will multiply N by a free parameter η that will be adjusted to fit experimental results.

Equations (5–7) can be solved numerically following the procedure described in Appendix A.

3.2. Dynamics of the laser

The dynamics of the laser depends strongly on how the different time scales associated with the evolutions of populations, coherences and field can be compared. Following the classification introduced in [76, 77], class A lasers are those in which population and polarization decay much faster than the field so that the dynamics is governed by the single field equation (for example He-Ne, Ar+, Kr+, dye lasers), class B lasers are those for which the population decays slowly and two equations are necessary (e.g.

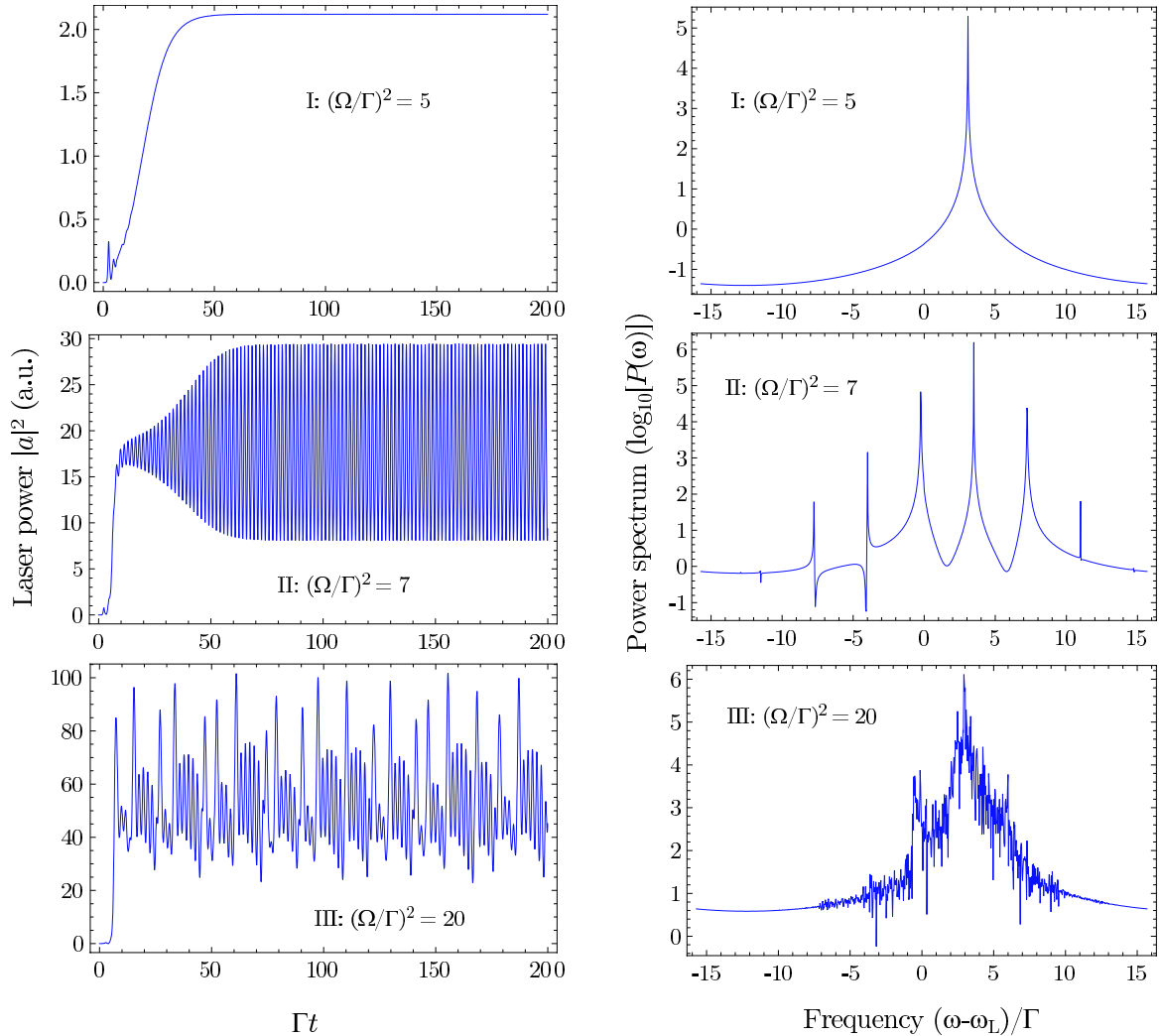


Figure 8. Laser power versus time (left) and corresponding power spectra (right) for the three different regimes of lasing: I – single-mode lasing, II – multi-mode lasing, and III – chaotic behaviour. The spectra are calculated in the stationary regime $\Gamma t > 100$. The parameters used in the calculation are the same as in figure 7.

ruby, Nd, CO₂ lasers) and finally, class C lasers are those for which the three time scales are of the same order of magnitude. The last ones are known to exhibit chaotic behaviour [76, 77].

For our cold atom sample, the relaxation rate of atomic coherences is only given by optical processes (no collision, e.g.). As a consequence, and with Mollow gain, the time scales for the evolution of the populations and coherences are both on the order of Γ^{-1} (note that this is not the case with Raman gain or FWM). The cavity damping rate κ is related to the finesse \mathcal{F} of the cavity by $\kappa = \pi c/2L\mathcal{F}$. With our experimental parameters, it gives $\kappa/2\pi \simeq 5.9$ MHz, i.e., $\kappa \sim \Gamma$ and we are thus

in a regime corresponding to class C lasers. This is consistent with the behaviour observed in our numerical simulation, as described in figures 7(b) and 8. We show the dependence of the laser power on the pump power in figure 7(b) for the case of when only a single mode ($M = 1$) with a well-defined frequency (detuning $\delta = 1.8\Gamma$) is present. The non-monotonic character of this dependence is accompanied by a complex dynamic behaviour that we illustrate in figure 8. Three distinct dynamic regimes are possible, depending on the pump strength: the laser emits at a single frequency (I) or at several frequencies at a time (II). In addition, chaotic behaviour appears for certain Ω (III). These results show that Mollow gain, associated to a low-finesse cavity, is perfectly suited for the study of chaotic regimes in lasers, as already predicted in [73].

We did not observe this kind of dependence of laser power as a function of the pump intensity in our experiment. This behaviour appears indeed only for some values of atom number or detuning δ_m and a specific experimental implementation would be needed. To model the experimental results, we solved the coupled laser equations with a well-defined single mode of the field ($M = 1$, detuning $\delta_1 = \delta$) and average the resulting laser intensity $|a|^2$ over 200 equidistant δ between -2Γ and 5Γ . This is supposed to account for the fact that the exact frequency of the cavity mode is not precisely known in the experiment and fluctuates shot to shot, as well as for averaging over many consecutive measurements (1000 in the experiment). Using η as a free parameter, we are then able to obtain a good fit to experimental data (solid line in figure 3). The obtained value of $\eta = 8$ is in qualitative agreement with the observation of high-order transverse laser modes: the corresponding cavity modes have a larger overlap with the atom cloud compared to a gaussian TEM₀₀ mode.

4. Threshold of a random laser with cold atoms

We now turn to the more specific question of realizing a *random* laser based upon one of the gain mechanisms studied in the previous section. As explained in the introduction, gain is not the only necessary ingredient for building a random laser, as scattering should also be present to provide feedback. In the previous laser experiment, scattering was not considered, and the optimum conditions for the laser operation are those which optimize the single-pass transmission through the cloud, which are very probably not the one that optimize scattering. To establish the best conditions for random lasing, we thus have to quantify more precisely the constraint of combining gain and scattering. This condition is already contained in the seminal Letokhov's paper [21], and leads indeed to the evaluation of the random laser threshold.

4.1. Random laser threshold

Although different kinds of random lasers have been achieved experimentally, several points are still under debate. Random lasers may be divided into two categories, depending on the feedback mechanism [37]. In the regime of incoherent (or intensity) transport, feedback is provided by an increase of the photon path lengths (or lifetime) in the system. This regime has been observed experimentally in many systems, such as powdered laser crystals [22], dye solutions containing microparticles [23], solid-states materials [38], or porous glass infiltrated by a dye solution in liquid crystal [26]. In a regime in which interference effects survive the random scattering process, a coherent (or field) feedback is expected, leading to a behaviour closer to that taking

place in conventional lasers. This behaviour is expected to become substantial close to the Anderson localization regime [34]. Experiments in this direction have been carried out, e.g., on zinc oxide powders [25, 37], and signatures of coherent feedback on the random lasing mechanism have been discussed recently [31, 32, 35]. For a given practical realization of a random laser, discriminating between a coherent or incoherent feedback mechanism is a complicated task. For example, narrow emission peaks above threshold can be observed, even far from the localization threshold [37, 78]. The existence of such peaks in experiments can be attributed to exponential gain along very long diffusion paths [78], or to interferences and coherent feedback in the weak scattering limit [31]. On the route towards a random laser with cold atoms, we first consider a diffusive random laser (with intensity feedback). This approach is motivated by the fact that experiments that should be carried out in the near future are expected to work in this regime. Another motivation is the identification of specific signatures of the incoherent feedback regime that could guide the experimental observations. A deviation from these signatures could be a measure of the onset of a coherent feedback mechanism.

4.2. Letokhov's threshold for cold atoms

From Letokhov's diffusive description of light transport in a homogeneous, disordered and active medium of size L , we know that the random laser threshold is governed by two characteristic lengths: the elastic scattering mean free path* ℓ_{sc} [79] and the linear gain length ℓ_g ($\ell_g < 0$ corresponds to absorption or inelastic scattering). In the diffusive regime, defined as $L \gg \ell_{sc}$, the lasing threshold is reached when the unfolded path length, on the order of L^2/ℓ_{sc} , becomes larger than the gain length. More precisely, the threshold is given by [21, 36]

$$L_{\text{eff}} > \beta\pi\sqrt{\ell_{sc}\ell_g/3}, \quad (8)$$

where β is a numerical factor that depends on the geometry of the sample ($\beta = 1$ for a slab, $\beta = 2$ for a sphere, which is the case we consider in the following), and $L_{\text{eff}} = \eta L$ is the effective length of the sample, taking into account the extrapolation length [79]. For $L > \ell_{sc}$ and a sphere geometry, $\eta = 1 + 2\xi/[L/\ell_{sc} + 2\xi]$ with $\xi \simeq 0.71$ [80, 81]. Note that deeply in the diffusive regime ($L \gg \ell_{sc}$), $\eta \sim 1$. Another important length scale is the extinction length ℓ_{ex} , as measured by the forward transmission of a beam through the sample, $T = e^{-L/\ell_{\text{ex}}}$. The extinction length is related to the other lengths by $\ell_{\text{ex}}^{-1} = \ell_{\text{sc}}^{-1} - \ell_g^{-1}$. Note that this reasoning may not be appropriate for backward gain such as produced by FWM.

For an atomic vapour, these characteristic lengths can both be computed as a function of the atomic polarizability $\alpha(\omega)$ at frequency ω . The extinction cross-section is indeed given by $\sigma_{\text{ex}}(\omega) = k \times \text{Im}[\alpha(\omega)]$ and the elastic scattering cross-section by $\sigma_{\text{sc}}(\omega) = k^4/6\pi \times |\alpha(\omega)|^2$ [82] ($k = \omega/c$ is the wave vector). Note that the first relation is general to any dielectric medium whereas the second one is specific to dipole scatterers. The characteristic lengths are then $\ell_{\text{ex,sc}}^{-1} = \rho\sigma_{\text{ex,sc}}$, where ρ is the atomic density. The gain cross-section can be defined the same way by $\ell_g^{-1} = \rho\sigma_g$. The vapour is supposed at constant density and homogeneously pumped, so that both ρ and α are position-independent. Even though this is not the precise geometry of a cold-atom

* We consider only isotropic scattering so that the transport length equals the scattering mean free path.

experiment, it allows us to perform analytical estimations. As we consider resonant scatterers, we deal only with quasi-resonant light and we shall use $k = k_0 = \omega_0/c$ with ω_0 the atomic eigenfrequency. In the following, we shall also use a dimensionless atomic polarizability $\tilde{\alpha}$, defined as $\alpha = \tilde{\alpha} \times 6\pi/k_0^3$, and omit the dependence on ω . We can now rewrite $\sigma_{\text{sc}} = \sigma_0|\tilde{\alpha}|^2$ and $\sigma_{\text{g}} = \sigma_0(|\tilde{\alpha}|^2 - \text{Im}(\tilde{\alpha}))$, where $\sigma_0 = 6\pi/k_0^2$ is the resonant scattering cross-section (for a $J = 0 \rightarrow J = 1$ transition), such that the threshold condition, as expressed by equation (8), reduces to [41]

$$\rho\sigma_0L_{\text{eff}} = \eta b_0 > \frac{2\pi}{\sqrt{3}|\tilde{\alpha}|^2 (|\tilde{\alpha}|^2 - \text{Im}(\tilde{\alpha}))}, \quad (9)$$

where b_0 is the on-resonance optical thickness of the cloud. This condition is valid as soon as the medium exhibits gain, i.e., $|\tilde{\alpha}|^2 - \text{Im}(\tilde{\alpha}) > 0$. Interestingly, the condition $\text{Im}(\tilde{\alpha}) < 0$, corresponding to single-pass amplification ($T > 1$), is not a necessary condition.

The threshold condition is thus given by a critical on-resonance optical thickness, which is an intrinsic parameter of the cloud, expressed as a function of the complex atomic polarizability only, which depends on the pumping parameters. Although the initial condition of equation (8) involves two characteristic lengths, we emphasize here that this is really one single independent parameter, as real and imaginary parts of the atomic polarizability are related via Kramers-Kronig relations [83]. This point is due to the originality of the system that we are considering, in which the same atoms are used to amplify and scatter light. This property can be fruitfully used to experimentally determine the threshold, as only one single measurement can provide enough information. A weak probe transmission spectrum, which we can rewrite with our notations,

$$T(\omega) = e^{-b_0 \text{Im}[\tilde{\alpha}(\omega)]}, \quad (10)$$

allows indeed the full characterization of $\tilde{\alpha}(\omega)$.

4.3. Application to Mollow and Raman gain

We now apply the previous results to Mollow gain and to Raman gain. For the first one we use the ab initio knowledge of the polarizability of a strongly pumped two-level atoms. For the second one, we use experimental transmission spectra $T(\omega)$ to extract the atomic polarizability via equation (10) and Kramers-Kronig relations.

With Mollow gain, the polarizability is exactly and analytically known [43], assuming a weak probe field, which is a good hypothesis for calculating the threshold of the random laser:

$$\begin{aligned} \tilde{\alpha}(\delta, \Delta, \Omega) = & -\frac{1}{2} \frac{1 + 4\Delta^2}{1 + 4\Delta^2 + 2\Omega^2} \\ & \times \frac{(\delta + i)(\delta - \Delta + i/2) - \Omega^2\delta/(2\Delta - i)}{(\delta + i)(\delta - \Delta + i/2)(\delta + \Delta + i/2) - \Omega^2(\delta + i/2)}, \end{aligned} \quad (11)$$

where Δ , δ and Ω are in unit of Γ .

For each pair of pumping parameters $\{\Delta, \Omega\}$, the use of the polarizability (11) into the threshold condition (9) allows the calculation of the critical on-resonance optical thickness b_0 as a function of the pump-probe detuning δ . Then, the minimum of b_0 and the corresponding δ determine the optical thickness $b_{0\text{cr}}$ that the cloud must overcome to allow lasing, and the frequency δ_{RL} of the random laser at threshold. The

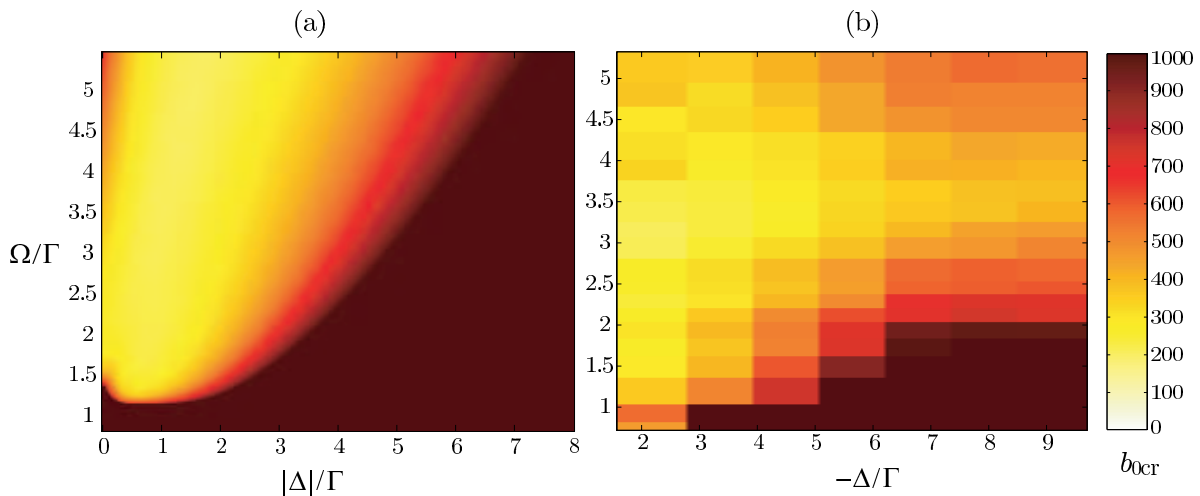


Figure 9. Threshold of random lasing based on Mollow gain (left) and Raman gain (right) for each pair of pumping parameters Δ (detuning) and Ω (Rabi frequency). We use the theoretical knowledge of the atomic polarizability (11) for Mollow gain whereas the prediction for Raman gain is based on experimental spectra (see text). In both cases, we obtain a minimum optical thickness of about 200.

result is presented in figure 9(a) for a spherical geometry ($\beta = 2$). The result for b_{0cr} is independent of the sign of Δ . The minimum optical thickness that allows lasing is found to be $b_{0cr} \approx 200$ and is obtained for a large range of parameters, approximately along the line $\Omega \approx 3\Delta$. The optimum laser-pump detuning is near the gain line of the transmission spectrum, i.e., $\delta_{RL} \sim \text{sign}(\Delta)\sqrt{\Delta^2 + \Omega^2}$, with however a small shift compared to the maximum gain condition due to the additional constraint of combined gain and scattering.

With Raman gain, we do not have a simple analytical expression of the polarizability. Nevertheless, we can measure its imaginary part by a transmission spectrum (equation (10)). A fit of the result, followed by its transformation by Kramers-Kronig relations [83], allows us to recover the full complex polarizability and to use equation (9) [42]. Note that this method is general and could be applied to any gain mechanism. However, Raman gain is perfectly suited for this analysis as we can fit the corresponding transmission profile by two inverted Lorentzian lines (see the Raman structure on figure 4(b), near $\delta = 0$), the transformation of which via Kramers-Kronig relations is analytic and well-known (it gives a standard dispersion profile). As the two Lorentzians are not well separated (for most parameters, $\delta_R < \gamma$), it leads for the scattering cross-section ($\propto |\tilde{\alpha}|^2$) to a bell-shaped curve centered near $\delta \sim 0$ [42]. Note that besides creating gain, the Raman transition *adds* some scattering.

As for Mollow gain, we have varied the pump parameters $\{\Delta, \Omega\}$ and for each pair, we have recorded a transmission spectrum and deduced the corresponding random laser threshold. We report the result on figure 9(b). The calculation contains corrections due to the peculiar polarization used in the experiment but deals only with the Raman resonance. It takes into account neither the main atomic absorption line at ω_0 (which adds elastic scattering), nor the losses due to inelastic scattering. Doing so, the two corrections almost compensate each other, and leads to $b_{0cr} \sim 200$

as the correct order of magnitude, obtained for $\Omega = \Delta \sim 3 - 4 \Gamma$ [42].

These results are very promising. Indeed, by using well-established techniques to compress magneto-optical traps (see, e.g., [84, 85]), achieving an optical thickness of 200 should not be too difficult.

4.4. Beyond the diffusive model

The calculation of the lasing threshold based on Lethokov's approach leads, for the optimum pumping parameters, to ratio $L/\ell_{sc} = b_{0cr}|\tilde{\alpha}|^2 \sim 0.5$ for Mollow gain and $L/\ell_{sc} \sim 2$ for Raman gain. Because these values are not consistent *a priori* with the domain of validity of the diffusion approximation, a more refined transport model is needed in order to check the relevance of the approach. A model for random lasers with incoherent feedback, going beyond the diffusion model, was introduced by Noginov *et al.* [86], based on a phenomenological one-dimensional modelling of light transport. In this work, we use a more advanced three-dimensional model based on the Radiative Transfer Equation (RTE), that was introduced as a tool to predict the threshold of "classical" random lasers [87], and that we extended recently to describe a cold-atom random laser with Mollow gain [41].

The RTE is a Boltzmann-type transport equation [88], that has a wider range of validity with respect to the ratio L/ℓ_{sc} than the diffusion equation [89]. The basic quantity is the specific intensity $I_\omega(\mathbf{r}, \mathbf{u}, t)$, which describes the number of photons at frequency ω , at point \mathbf{r} , propagating along direction \mathbf{u} at time t . In order to compare the diffusive and RTE predictions, we will consider a slab geometry, with the z axis normal to the slab surfaces. In the case of plane-wave illumination at normal incidence, and for isotropic scatterers, the specific intensity only depends on the space variable z and the angular variable $\mu = \cos\theta$, with θ the angle between the propagation direction \mathbf{u} and the z -axis. In a system exhibiting gain and (isotropic) scattering, the RTE reads:

$$\frac{1}{c} \frac{\partial I_\omega}{\partial t}(z, \mu, t) + \mu \frac{\partial I_\omega}{\partial z}(z, \mu, t) = (\ell_g^{-1} - \ell_{sc}^{-1}) I_\omega(z, \mu, t) + (2\ell_{sc})^{-1} \int_{-1}^{+1} I_\omega(z, \mu', t) d\mu' \quad (12)$$

where c is the energy velocity in the medium.

A feature of the RTE is that a modal expansion is available, whose asymptotic behaviour at large length and time scales leads to the modal expansion of the diffusion equation [80]. Therefore, under the conditions of uniform (in space) and constant (in time) gain, it is possible to build a modal theory of random lasers with incoherent feedback based on the RTE, that generalizes Lethokov's approach beyond the diffusive regime [87]. We focus on the slab geometry ($\beta = 1$) since the modal expansion of the RTE is well known in this case [80] (to our knowledge, no simple expansion is available for a sphere in the RTE approach). The modal approach consists in looking for solutions of the form $I(z, \mu, t) = I_{\kappa,s}(\mu) \exp(i\kappa z) \exp(st)$, where $I(z, \mu, t)$ is the specific intensity and the dependence on ω has been omitted for simplicity. κ can be chosen as a real parameter, and s can take complex values. For a given real κ , $s(\kappa)$ and $I_{\kappa,s}$ form a set of eigenvalues and eigenfunctions of the RTE. For isotropic scattering, eigenvalues and eigenfunctions can be obtained analytically [80]. In a passive medium,

the eigenvalue corresponding to the mode with the longest lifetime reads \ddagger :

$$s_0(\kappa)/c = \ell_g^{-1} - [\ell_{sc}^{-1} - \kappa/\tan(\kappa \ell_{sc})] , \text{ for } \kappa \ell_{sc} < \frac{\pi}{2} . \quad (13)$$

In the presence of gain, the lasing threshold is reached when this modes starts to display an exponential amplification in time. Determining the threshold parameters amounts to calculating the gain length and scattering mean free path generating an eigenvalue $s_0(\kappa) > 0$. Exactly at threshold, one has $s_0(\kappa) = 0$. For a slab of width L , the dominant mode corresponds to $\kappa = \pi/L_{\text{eff}} = \pi/(L + 2\xi\ell_{sc})$. In practice, the determination of κ is meaningful as long as $\xi = 0.71$ can be taken as a constant (independent on L). Although not shown for brevity, we have verified with a full numerical solution of the RTE that this is the case as soon as $L > \ell_{sc}$. This condition sets a limit of accuracy of the modal approach.

It is well known that the diffusion approximation is asymptotically reached from the RTE in the limit of long time and large length scales. Indeed, in the limit $\kappa\ell_{sc} \ll 1$, a first-order expansion of equation (13) yields

$$s_0^{(\text{DA})}(\kappa)/c = \ell_g^{-1} - \kappa^2\ell_{sc}/3, \quad (14)$$

which is the dispersion relation of the modes of the diffusion equation (DA) [80, 90]. The associated threshold condition $s_0^{(\text{DA})}(\kappa = \pi/L_{\text{eff}}) = 0$ corresponds exactly to the result obtained with Letokhov's approach, with $\beta = 1$. A careful look at equations (13) and (14) shows that the predictions of the RTE and diffusion approximation should not be substantially different. Firstly, we note that the gain contribution to $s_0(\kappa)$ is the same in both models (the first term is the same in equations (13) and (14)). Secondly, the scattering contribution (the second term in the equations) is larger in the RTE model, but by a factor that remains smaller than 1.13 (when $L \sim \ell_{sc}$). This means that the correction introduced by the RTE remains relatively small, at least for the slab geometry. Numerically, it corresponds to an increase of $\eta b_{0\text{cr}}$ of at most a few percents [41]. We can conclude that the model based on the diffusion approximation gives accurate results, even in the regime $L \sim \ell_{sc}$. Also note that the accuracy should be better with Raman gain, for which the optimum conditions are reached for $L/\ell_{sc} \sim 2$ (instead of $L/\ell_{sc} \sim 0.5$ for Mollow gain). Finally, we stress that our prediction shows that in a cold-atom system, random lasing could be achieved even in a regime of low scattering. This is a feature of a system exhibiting a high level of gain, in which the threshold can be reached even with a low-quality feedback (i.e., a cavity with a poor quality factor).

4.5. Emitted intensity above threshold

In this section we focus on the characterization of the Mollow random laser above threshold. The threshold of a random laser with Mollow gain can be predicted using the lasing condition (9) together with the polarizability given by equation (11). This polarizability is obtained in the weak probe limit [43]. When the lasing threshold is surpassed, Letokhov's theory leads to an exponential growth of the laser intensity versus time, and hence steady state cannot be reached. In order to avoid this unphysical effect, as already pointed in [21], saturation effects must be included in the description of the atomic polarizability at both pump and probe frequencies.

\ddagger Note that a misprint occurred in the published version of [41] and that the correct expression is given here.

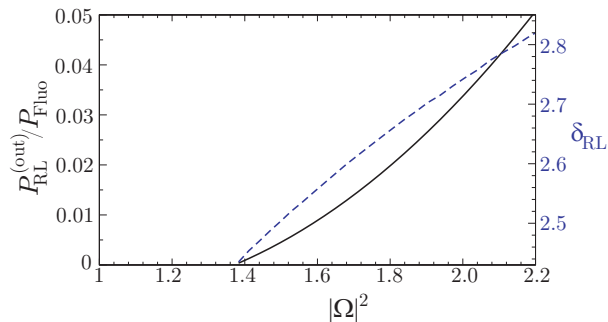


Figure 10. Continuous line: Emitted random laser power normalized to the pump fluorescence power, as a function of the pump intensity. Dashed line: Normalized laser detuning δ_{RL} . The random medium is a spherical cloud of two level atoms with an on-resonance optical-thickness $b_0 = 600$.

To do so, optical Bloch equations in the strong probe regime can be numerically solved in order to obtain the atomic polarizability. In this case the atomic polarizability depends on the lasing intensity in the medium $I_{\text{RL}}^{(\text{in})}$ through its associated Rabi frequency $|\Omega_{\text{RL}}|^2 \propto I_{\text{RL}}^{(\text{in})}$. Hence, $\tilde{\alpha} = \tilde{\alpha}(\delta, \Delta, \Omega, \Omega_{\text{RL}})$ (all frequencies will be in unit of Γ in the following equations). The steady-state value of the random laser Rabi frequency is considered as the value at which losses exactly compensate gain. In this situation, the output power of the random laser $P_{\text{RL}}^{(\text{out})}$ equals the generated power in the lasing medium, i.e., $P_{\text{RL}}^{(\text{out})} \propto \sigma_{\text{g}} |\Omega_{\text{RL}}|^2$, with $\sigma_{\text{g}} = \sigma_0 (|\tilde{\alpha}|^2 - \text{Im}(\tilde{\alpha}))$ the gain cross-section. On the other hand, the pump-induced fluorescence power is $P_{\text{Fluo}} \propto \sigma_0 |\Omega|^2 / (1 + 4\Delta^2 + 2|\Omega|^2)$.

Hence, in this regime the ratio of the lasing power to the fluorescence power induced by the pump can be estimated. This ratio is an important step towards the performance characterization of the random laser, as it allows to quantify the amount of laser signal that can be extracted from the fluorescence background. From the previous results we get

$$\frac{P_{\text{RL}}^{(\text{out})}}{P_{\text{Fluo}}} = \frac{|\Omega_{\text{RL}}|^2}{|\Omega|^2} (|\tilde{\alpha}|^2 - \text{Im}(\tilde{\alpha})) (1 + 4\Delta^2 + 2|\Omega|^2) . \quad (15)$$

As can be seen in figure 10, the ratio of lasing power to fluorescence background is on the order of 5% for a pump detuning $\Delta = 1$, leading to a measurable signal. One interesting characteristic of this random laser concerns the laser frequency at its maximum emission power. As shown in figure 10, this maximum emission frequency shifts as the pump intensity increases. This effect is due to the shift in the Mollow gain as the pumping power changes.

4.6. Limitations of the model

Of course these crude estimations neglect different effects. We assume homogeneous pump intensity across the whole system [86]. We are considering one pump frequency and one lasing frequency, neglecting thus effects resulting from mode competition [32] and inelastic scattering of laser light [91] among others. Despite neglecting those

effects, these estimations seem to be reasonable at least in recovering the orders of magnitude of the lasing threshold and power.

The inhomogeneities in the atomic cloud density, in the pump intensity and in the gain distributions could be incorporated in the RTE model, at the cost of a full numerical treatment of coupled equations for the pump beam and emitted light intensities. Such an approach has been developed previously in the case of a “classical” random laser, i.e., with gain and scattering as separate entities [87]. Another improvement would be to deal with a spherical geometry, that is closer to the real conditions. Finally, including the Raman gain mechanism into the RTE approach, using experimental data as input parameters, would be of great interest in view of experiments since the threshold conditions seem easier to reach than with Mollow gain, in view of our first estimates.

5. Outlook and conclusion

We have presented in this paper our recent investigations on the issue of achieving a diffusive random laser in a cloud of cold atoms. We have especially studied different gain mechanisms in a situation of standard laser, and we have quantified the random laser threshold for two of them. These evaluations show that random laser in cold atoms *is possible*. This is undoubtedly our main result. Moreover, we point out that the peculiarity of our system would lead to a random laser with a low amount of scattering, that is, low feedback. This regime is similar to that encountered in certain semiconductor lasers with a very poor cavity, and is different from the working regime of random lasers realized to date.

Moreover, from our experience, we can now draw some preliminary conclusions about the comparison of the different gain mechanisms. Application of Letokhov’s criteria leads to similar critical optical thickness for Mollow gain and Raman gain. Nevertheless, the optimum for Mollow gain is obtained outside the range of validity of our transport model whereas the amount of scattering is larger with Raman gain. Moreover, polarization is better taken into account in our prediction for Raman gain. Finally, the optimum pumping parameters are such that pump penetration through the cloud will be higher with Raman gain, since detuning and power are larger. For all these reasons, Raman gain seems more appropriate to achieve random lasing.

However, achieving random lasing is not enough, as we need also to *detect* the random laser emission. In our system, gain is almost at the same wavelength than the pump (and thus its fluorescence), and this makes the detection challenging. In this respect, Raman gain is worse than Mollow gain, as the very small detuning δ_R between the pump and the gain frequency prevent the use of a Fabry-Perot interferometer to distinguish between the laser emission and the pump-induced fluorescence. This could be done more easily with Mollow gain (see, e.g., [92]). Moreover, from our preliminary evaluations of the intensity of the random laser emission with Mollow gain (section 4.5), we know that the random laser emission should not be too small to be detected.

For Raman gain we can imagine other ways to extract the optical spectrum of the emitted light, by looking at the intensity correlations of the fluorescence, measured by a heterodyne technique [93] or a homodyne technique [94] or a correlator [95]. Nevertheless it does not allow to filter the light, contrary to the Fabry-Perot technique. Filtering the random laser light could be very useful to study the random laser properties, for example the intensity temporal correlations. Note that this kind of experiments could be interesting also below the random laser threshold [96, 97].

The third gain mechanism that we have studied is four-wave mixing, which has lead to a very efficient cavity-laser. Nevertheless, the configuration we have used so far, that is *degenerate* FWM, is not appropriate at all for the random laser problem, as the pump fluorescence and the random laser emission would be exactly at the same frequency. However, another configuration of parametric gain is possible, that is non-degenerate FWM, for which two different frequencies ω_F and ω_B are used for the two pump fields, and amplification occurs at frequency $\omega = (\omega_F + \omega_B)/2$. Then, it should be possible to choose a large enough detuning to facilitate the detection, and to adjust the gain frequency close to the atomic frequency ω_0 to enhance scattering. Preliminary numerical simulations indicate that this configuration is promising [98], and its experimental test constitutes our next work.

Finally, we may also use some extra degrees of freedom that atoms offer, for example the use of magnetic fields to engineer the multiple scattering properties of atoms [99, 100] to better control the random laser based on cold atoms.

Acknowledgments

This work is supported by ANR CAROL (project ANR-06-BLAN-0096). L.S.F. acknowledges the financial support of Spanish ministry of science and innovation through its Juan de la Cierva program, D.B. acknowledges support from INTERCAN, N.M. and F.M. are funded by DGA.

Appendix A. Laser dynamics equations

We give here the expressions of the functions Φ , Ψ and Θ that describe the coupling terms in the laser dynamics coupled equations (5–7) [73, 74]:

$$\Phi(\sigma_j, a_m) = 2i\lambda_1 \sum_{m=1}^M (\exp[-i\phi_j]\sigma_j a_m^* - \exp[i\phi_j]\sigma_j^* a_m) \quad (\text{A.1})$$

$$+ 2i\lambda_2 \sum_{m=1}^M (\exp[-i\phi_j]\sigma_j^* a_m^* - \exp[i\phi_j]\sigma_j a_m) + 2\gamma_3 (\sigma_j + \sigma_j^*) ,$$

$$\Psi(\sigma_j, \sigma_{3j}, a_m) = -i \sum_{m=1}^M (\exp[i\phi_j]\lambda_1 \sigma_{3j} a_m + \exp[-i\phi_j]\lambda_2 \sigma_{3j} a_m^*) \quad (\text{A.2})$$

$$- 2i\lambda_0 \sum_{m=1}^M (\exp[-i\phi_j]\sigma_j a_m^* + \exp[i\phi_j]\sigma_j a_m) + \gamma_0 + \gamma_3 \sigma_{3j} - \gamma_4 \sigma_j^* ,$$

$$\Theta(\sigma_{3j}, \sigma_j) = -i \sum_{j=1}^N \exp[-i\phi_j] (\lambda_1 \sigma_j - \lambda_2 \sigma_j^* + \lambda_0 \sigma_{3j}) , \quad (\text{A.3})$$

where $\gamma_0 = (\Gamma/2) \sin 2\theta$, $\gamma_3 = (\Gamma/4) \sin 2\theta \cos 2\theta$, $\gamma_4 = (\Gamma/4) \sin^2 2\theta$, $\lambda_0 = (g/4) \sin 2\theta$, $\lambda_1 = (g/4) (1 + \cos 2\theta)$ and $\lambda_2 = (g/4) (1 - \cos 2\theta)$.

The procedure to numerically solve the equations (5–7) follows the method presented in [73]. We introduce a family of n -photon polarizations $S_n = \sum_j \exp[-in\phi_j]\sigma_j$ and $S_{3n} = \sum_j \exp[-in\phi_j]\sigma_{3j}$. Equations (5,6) cast then into an infinite set of hierarchical equations for S_n and S_{3n} . In this paper, we truncate this set of equations at $|n| = 5$, which, in the case of $M = 1$, leaves us with a total of

35 equations and corresponds to the generalized effective theory GET35, if we use terminology of [73]. The hierarchical equations for macroscopic polarizations S_n and S_{3n} , supplemented with equations for amplitudes of modes a_m of the electromagnetic field, are then solved numerically.

References

- [1] Cohen-Tannoudji C, Dupont-Roc J and Grynberg G 1992 *Atom-Photon Interactions: Basic Processes and Applications* (New York: Wiley)
- [2] Holstein T 1947 *Phys. Rev.* **72** 1212–1233
- [3] Molisch A and Oehry B 1998 *Radiation Trapping in Atomic Vapours* (Oxford University Press)
- [4] Metcalf H and van der Straten P 1999 *Laser cooling and Trapping* (New York: Springer)
- [5] Fioretti A, Molisch A F, Mütter J H, Verkerk P and Allegrini M 1998 *Opt. Commun.* **149** 415–422
- [6] Labeyrie G, Vaujour E, Müller C A, Delande D, Miniatura C, Wilkowski D and Kaiser R 2003 *Phys. Rev. Lett.* **91** 223904
- [7] Labeyrie G, Kaiser R and Delande D 2005 *Appl. Phys. B* **81** 1001–1008
- [8] Labeyrie G, de Tomasi F, Bernard J C, Müller C A, Miniatura C and Kaiser R 1999 *Phys. Rev. Lett.* **83** 5266–5269
- [9] Bidet Y, Klappauf B, Bernard J C, Delande D, Labeyrie G, Miniatura C, Wilkowski D and Kaiser R 2002 *Phys. Rev. Lett.* **88** 203902
- [10] Kaiser R and Havey M D 2005 *Opt. Photon. News* **16** 38–43
- [11] Kupriyanov D V, Sokolov I M, Sukenik C I and Havey M D 2006 *Laser Phys. Lett.* **3** 223–243
- [12] Labeyrie G 2008 *Mod. Phys. Lett. B* **22** 73–99
- [13] Aegerter C M and Maret G 2009 *Progress in Optics* vol 52 ed E. Wolf (Amsterdam, North-Holland: Elsevier) pp 1–61
- [14] Grynberg G and Robillard C 2001 *Phys. Rep.* **355** 335–451
- [15] Tabosa J W R, Chen G, Hu Z, Lee R B and Kimble H J 1991 *Phys. Rev. Lett.* **66** 3245–3248
- [16] Grison D, Lounis B, Salomon C, Courtois J Y and Grynberg G 1991 *Europhys. Lett.* **15** 149–154
- [17] Hilico L, Fabre C and Giacobino E 1992 *Europhys. Lett.* **18** 685–688
- [18] Miller R, Northup T E, Birnbaum K M, Boca A, Boozer A D and Kimble H J 2005 *J. Phys. B: At. Mol. Opt. Phys.* **38** S551–S565
- [19] Kruse D, von Cube C, Zimmermann C and Courteille P W 2003 *Phys. Rev. Lett.* **91** 183601
- [20] Guerin W, Michaud F and Kaiser R 2008 *Phys. Rev. Lett.* **101** 093002
- [21] Letokhov V S 1968 *Sov. Phys. JETP* **26** 835–840
- [22] Gouedard C, Husson D, Sauteret D, Auzel F and Migus A 1993 *J. Opt. Soc. Am. B* **10** 2358–2362
- [23] Lawandy N M, Balachandran R M, Gomes A S L and Sauvain E 1994 *Nature* **368** 436–438
- [24] Cao H, Zhao Y G, Ong H C, Ho S T, Dai J Y, Wu J Y and Chang R P H 1998 *Appl. Phys. Lett.* **73** 3656–3658
- [25] Cao H, Zhao Y G, Ho S T, Seelig E W, Wang Q H and Chang R P H 1999 *Phys. Rev. Lett.* **82** 2278–2281
- [26] Wiersma D S and Cavalier S 2001 *Nature* **414** 708–709
- [27] Strangi G, Ferjani S, Barna V, Luca A D, Versace C, Scaramuzza N and Bartolino R 2006 *Opt. Express* **14** 7737–7744
- [28] Gottardo S, Sapienza R, García P D, Blanco A, Wiersma D S and López C 2008 *Nature Photon.* **2** 429–432
- [29] Wiersma D S and Lagendijk A 1996 *Phys. Rev. E* **54** 4256–4265
- [30] Burin A L, Ratner M A, Cao H and Chang R P H 2001 *Phys. Rev. Lett.* **87** 215503
- [31] Vanneste C, Sebbah P and Cao H 2007 *Phys. Rev. Lett.* **98** 143902
- [32] Türeci H E, Ge L, Rotter S and Stone A D 2008 *Science* **320** 643–646
- [33] Wiersma D S 2008 *Nature Phys.* **4** 359–367
- [34] Anderson P W 1958 *Phys. Rev.* **109** 1492–1505
- [35] Conti C and Fratallocchi A 2008 *Nature Phys.* **4** 794–798
- [36] Cao H 2003 *Waves Random Media* **13** R1–R39
- [37] Cao H 2005 *J. Phys. A: Math. Gen.* **38** 10497–10535
- [38] Noginov M 2005 *Solid-State Random Lasers* (Berlin: Springer)
- [39] Bonifacio R and Lugiato L A 1975 *Phys. Rev. A* **11** 1507–1521
- [40] Paradis E, Barrett B, Kumarakrishnan A, Zhang R and Raitzel G 2008 *Phys. Rev A* **77** 043419
- [41] Froufe-Pérez L S, Guerin W, Carminati R and Kaiser R 2009 *Phys. Rev. Lett.* **102** 173903

- [42] Guerin W, Mercadier N, Brivio D and Kaiser R 2009 *Opt. Express* in press (Preprint arXiv:0903.5190)
- [43] Mollow B R 1972 *Phys. Rev. A* **5** 2217–2222
- [44] Wu F Y, Ezekiel S, Ducloy M and Mollow B R 1977 *Phys. Rev. Lett.* **38** 1077–1080
- [45] Grynberg G and Cohen-Tannoudji C 1993 *Opt. Commun.* **96** 150–163
- [46] Grandclément D, Grynberg G and Pinard M 1987 *Phys. Rev. Lett.* **59** 40–43
- [47] Zakrzewski J 1992 *Phys. Rev. A* **46** 6010–6014
- [48] Mompert J and Corbalán R 2000 *J. Opt. B: Quantum Semiclass. Opt.* **2** R7–R24
- [49] Brzozowski T M, Brzozowska M, Zachorowski J, Zawada M and Gawlik W 2005 *Phys. Rev. A* **71** 013401
- [50] Yariv A and Pepper D M 1977 *Opt. Lett.* **1** 16–18
- [51] Abrams R L and Lind R C 1978 *Opt. Lett.* **2** 94–96
Abrams R L and Lind R C 1978 *Opt. Lett.* **3** 205
- [52] Boyd R W, Raymer M G, Narum P and Harter D J 1981 *Phys. Rev. A* **24** 411–423
- [53] Kleinmann B, Trehin F, Pinard M and Grynberg G 1985 *J. Opt. Soc. Am. B* **2** 704–713
- [54] Pinard M, Grandclément D and Grynberg G 1986 *Europhys. Lett.* **2** 755–760
- [55] Leite M R R, Simoneau P, Bloch D, Le Boiteux S and Ducloy M 1986 *Europhys. Lett.* **2** 747–753
- [56] Michaud F, Gattobigio G L, Tabosa J W R and Kaiser R 2007 *J. Opt. Soc. Am. B* **24** A40–A47
- [57] Lind R C and Steel D G 1981 *Opt. Lett.* **6** 554–556
- [58] Grynberg G, Maître A and Petrossian A 1994 *Phys. Rev. Lett.* **72** 2379–2383
- [59] Ackemann T and Lange W 2001 *App. Phys. B* **72** 21–34
- [60] Vallet M, Pinard M and Grynberg G 1990 *Europhys. Lett.* **11** 739–744
- [61] McCormick C F, Boyer V, Arimondo E and Lett P D 2007 *Opt. Lett.* **32** 178–180
- [62] Boyer V, Marino A M, Pooser R C and Lett P D 2008 *Science* **321** 544–547
- [63] Gattobigio G L, Michaud F, Javaloyes J, Tabosa J W R and Kaiser R 2006 *Phys. Rev. A* **74** 043407
- [64] Kumar P and Shapiro J H 1985 *Opt. Lett.* **10** 226–228
- [65] Padmabandu G G, Welch G R, Shubin I N, Fry E S, Nikonov D E, Lukin M D and Scully M O 1996 *Phys. Rev. Lett.* **76** 2053–2056
- [66] Zibrov A S, Lukin M D, Nikonov D E, Hollberg L, Scully M O, Velichansky V L and Robinson H G 1995 *Phys. Rev. Lett.* **75** 1499–1502
- [67] Kitching J and Hollberg L 1999 *Phys. Rev. A* **59** 4685–4689
- [68] Courtois J Y, Grynberg G, Lounis B and Verkerk P 1994 *Phys. Rev. Lett.* **72** 3017–3020
- [69] Vengalattore M and Prentiss M 2005 *Phys. Rev. A* **72** 021401
- [70] Bonifacio R and Salvo L D 1994 *Nucl. Instrum. Methods Phys. Res. Sect. A* **341** 360 – 362
- [71] Berman P R 1999 *Phys. Rev. A* **59** 585–596
- [72] Gauthier D J, Wu Q, Morin S E and Mossberg T W 1992 *Phys. Rev. Lett.* **68** 464–467
- [73] Zakrzewski J and Lewenstein M 1992 *Phys. Rev. A* **45** 2057–2069
- [74] Zakrzewski J, Lewenstein M and Mossberg T W 1991 *Phys. Rev. A* **44** 7717–7731
Zakrzewski J, Lewenstein M and Mossberg T W 1991 *Phys. Rev. A* **44** 7732–7745
Zakrzewski J, Lewenstein M and Mossberg T W 1991 *Phys. Rev. A* **44** 7746–7758
- [75] Mu Y and Savage C M 1992 *Phys. Rev. A* **46** 5944–5954
- [76] Arecchi F T, Lippi G L, Puccioni G P and Tredicce J R 1984 *Opt. Commun.* **51** 308–314
- [77] Tredicce J R, Arecchi F T, Lippi G L and Puccioni G P 1984 *J. Opt. Soc. Am. B* **2** 173–183
- [78] Mujumdar S, Ricci M, Torre R and Wiersma D S 2004 *Phys. Rev. Lett.* **93** 053903
- [79] van Rossum M C W and Nieuwenhuizen T M 1999 *Rev. Mod. Phys.* **71** 313–371
- [80] Case K and Zweifel P 1967 *Linear transport theory* (Reading, MA: Addison-Wesley)
- [81] Drozdowicz K, Krynicka E and Dąbrowska J 2003 *App. Rad. Isot.* **58** 727–733
- [82] Lagendijk A and van Tiggelen B A 1996 *Phys. Rep.* **270** 143–215
- [83] Jackson J D 1999 *Classical Electrodynamics* 3rd ed (New York: Wiley)
- [84] Ketterle W, Davis K B, Joffe M A, Martin A and Pritchard D E 1993 *Phys. Rev. Lett.* **70** 2253–2256
- [85] dePue M T, Winoto S L, Han D J and Weiss D S 2000 *Opt. Commun.* **180** 73–79
- [86] Noginov M A, Novak J, Grigsby D and Deych L 2006 *J. Opt. A: Pure Appl. Opt.* **8** S285–S295
- [87] Pierrat R and Carminati R 2007 *Phys. Rev. A* **76** 023821
- [88] Chandrasekhar S 1960 *Radiative Transfer* (New York: Dover)
- [89] Elaloufi R, Carminati R and Greffet J J 2004 *J. Opt. Soc. Am. B* **21** 1430–1437
- [90] Pierrat R, Greffet J J and Carminati R 2006 *J. Opt. Soc. Am. A* **23** 1106–1110
- [91] Khaykovich L, Friedman N and Davidson N 1999 *Eur. Phys. J. D* **7** 467–473
- [92] Wu F Y, Grove R E and Ezekiel S 1975 *Phys. Rev. Lett.* **35** 1426–1429
- [93] Westbrook C I, Watts R N, Tanner C E, Rolston S L, Phillips W D, Lett P D and Gould P L

- 1990 *Phys. Rev. Lett.* **65** 33–36
- [94] Jurczak C, Sengstock K, Kaiser R, Vansteenkiste N, Westbrook C I and Aspect A 1995 *Opt. Commun.* **115** 480–484
- [95] Bali S, Hoffmann D, Simán J and Walker T 1996 *Phys. Rev. A* **53** 3469–3472
- [96] Yamilov A, Chang S-H, Burin A, Taflove A and Cao H 2005 *Phys. Rev. B* **71** 092201
- [97] Fedorov V Y and Skipetrov S E 2009 *Preprint* arXiv:0904.3696
- [98] Mercadier N 2008 *Diffusion à Résonance Atomique: application au mélange à 4 ondes et au vol de Lévy du photon* Master Thesis, Ecole Centrale de Paris
- [99] Labeyrie G, Miniatura C, Müller C A, Sigwarth O, Delande D and Kaiser R 2002 *Phys. Rev. Lett.* **89** 163901
- [100] Sigwarth O, Labeyrie G, Jonckheere T, Delande D, Kaiser R and Miniatura C 2004 *Phys. Rev. Lett.* **93** 143906